SpherePHD: Applying CNNs on a Spherical PolyHeDron Representation of 360° Images

Yeon Kun Lee* Jaeseok Jeong* Jong Seob Yun* Won June Cho Kuk-Jin Yoon

{dldusrjs, jason.jeong, jseob, wonjune, kjyoon}@kaist.ac.kr Visual Intelligence Lab., Department of Mechanical Engineering, KAIST, Korea

Abstract

Omni-directional cameras have many advantages over conventional cameras in that they have a much wider field-of-view (FOV). Several approaches have been recently proposed to apply convolutional neural networks (CNNs) to omni-directional images to solve classification and detection problems. However, most of them use image representations in the Euclidean space defined by transforming the omni-directional views originally in the non-Euclidean space. This transformation leads to shape distortion due to nonuniform spatial resolving power and loss of continuity. These effects make existing convolution kernels have difficulties in extracting meaningful information.

This paper proposes a novel method to resolve the aforementioned problems of applying CNNs to omni-directional images. The proposed method utilizes a spherical polyhedron to represent omni-directional views. This method minimizes the variance of spatial resolving power on the sphere surface, and includes new convolution and pooling methods for the proposed representation. The proposed approach can also be adopted by existing CNN-based methods. The feasibility and efficacy of the proposed method is demonstrated through both classification and detection tasks.

1. Introduction

 360° cameras have many advantages over traditional cameras in the fact that they offer an omni-directional view of the scene rather than a narrow field of view. This omnidirectional view of 360° cameras ¹ allows us to extract more information from the scene at once. Therefore, 360° cameras can play an important role in systems requiring rich information of its surroundings, *e.g.* advanced driver assistance systems (ADAS), and autonomous robotics.

Meanwhile, convolutional neural networks (CNNs) have



Figure 1. Spatial distortion due to nonuniform spatial resolving power in an ERP image. Yellow squares on both sides represent the same surface areas on the sphere.

been widely used for many visual tasks to preserve locality information. They have shown great accuracy in classification and detection problems as in [8] [11] [13] [14].

Following this trend, several approaches have been recently proposed to apply CNNs to omni-directional images to solve classification and detection problems. Since the input data of neural networks are usually represented in the Euclidean space, it is required to represent the omni-directional images in Euclidean space, even though omni-directional images are originally represented in non-Euclidean polar coordinates. To this end, equi-rectangular projection (ERP) has been commonly used to represent omni-directional images in regular grids.

However, there exist spatial distortion in ERP images coming from the nonuniform spatial resolving power, which is caused by the non-linearity of the transformation as shown in Fig. 1. This effect is more severe near the poles. In addition, another distortion is observable when the omnidirectional image is taken by tilting the 360° camera. In this case, without adjusting for the camera tilting angle, ERP introduces a sinusoidal fluctuation of the horizon as in Fig. 2. This in return distorts the image, making the task of visual perception much more difficult.

In conventional 2D images, the regular grids along vertical and horizontal directions allow the convolution domain to be uniform; the uniform domain enables the same shaped

^{*}These authors contributed equally

^{1&#}x27;360°' and 'omni-directional' are used interchangeably in the paper.





Figure 2. Problems of using ERP images. (left) When an omnidirectional image is taken by a tilted camera, a sinusoidal fluctuation of the horizon occurs in the ERP image. The yellow dotted line represents the fluctuating horizon [1]. (right) When the car is split, the car is detected as cars with two different IDs . This image is from SUN360 dataset [22] to demonstrate effects of edge discontinuity.

kernels to represent the image convolution over the whole image. However, in ERP images, the nonuniform spatial resolving power as shown in Fig. 1 and Fig. 2(left) causes the convolution domain to vary over the ERP image, making the same shaped kernels inadequate for the ERP image convolution.

Furthermore, during the transformation from the non-Euclidean space to the Euclidean space, some important properties can be lost. For example, the non-Euclidean space that omni-directional images are defined in has a cyclical property: unidirectional translation along a sphere surface (*i.e.* in an omni-directional image) is always continuous and returns to the starting point eventually. However, during the transformation from the non-Euclidean space to the Euclidean space through the ERP, the continuity and cyclical properties are lost. This causes a discontinuity along the borders of the ERP image. The discontinuity can cause a single object to be misinterpreted in detection problems as two different objects when the object is split in half by the borders as shown in Fig. 2(right).

Recently, there has been an attempt to keep the continuity of the omni-directional image by projecting the image onto a cube map [12]. Projecting an omni-directional image onto a cube map also has the benefit that the spatial resolving power in an image varies much less compared with ERP images. Furthermore, the performance of cube map representation is less affected by rotation than ERP representation. As a result, projecting a spherical image onto a cube map has shown improvements from using ERP for omnidirectional images, but it still has some flaws. For example, during the transformation, the image resolving power varies from the centers of the faces to their edges. This will be illustrated in Sec. 4.

In this paper, we propose a new representation of omnidirectional images followed by new convolution and pooling methods to apply CNNs based on the proposed representation. As an attempt to reduce the variance of spatial resolving power in representing the 360° images, we come up with a spherical polyhedron-based representation of images (SpherePHD). Utilizing the properties of a SpherePHD constructed by an icosahedral geodesic polyhedron, we present a geometry where an omni-directional image can be projected onto. The proposed projection will give less variance of spatial resolving power and distortion than others. Furthermore, the rotational symmetry of the spherical geometry will allow the image processing algorithms to be rotation invariant. Lastly, the spherical polyhedron provides a continuity property; there is no border where the image becomes discontinuous. This particular representation aims to resolve both the issues raised in using ERP and cube map representations. The contributions of this paper also include designing the convolution kernel and a specific method of applying convolution kernels and pooling kernels to use CNNs on the proposed spherical polyhedron representation of images. In order to show that the newly proposed method is superior to ERP and cube map representations, we compare classification and detection accuracies based on the different representations. To conduct comparison experiments, we have also created a spherical MNIST dataset and spherical SYNTHIA dataset [15] through spherical polyhedron projection of the datasets. The datasets and source codes for our method is available at http://.

2. Related works

In this section, we will discuss relevant works that have been done for CNNs on omni-directional images.

2.1. ERP-based methods

As mentioned earlier, an ERP image has its flaws: the nonuniform spatial resolving power brings about distortion effects, the image has rotational constraints, and the image lacks continuity at the borders. Yang et al. [20] compared the results of different detection algorithms that take ERP images directly as inputs, showing that not solving the distortion problem still produces a relevant accuracy. Other papers proposed to remedy the flaws of the ERP based method. To tackle the issue of nonuniform resolving power, Coors et al. [5] proposed sampling pixels from the ERP image, in a rate dependent on latitude, to preserve uniform spatial resolving power to keep the convolution domain consistent in each kernel. Hu et al. [7] and Su and Grauman [17] partitioned the omni-directional image into subimages and produced normal field of view (NFoV) images; during the partitioning stages, they also reduced the distortion effects in the ERP image. Lai et al. [9] and Su et al. [18] generated saliency maps from omni-directional images and extracted specific NFoV images from areas of high saliency. The use of NFoV image sampling increased accuracy by solving the distortion problem, but extracting NFoV images from an omni-directional image is not as beneficial as utilizing the whole omni-directional view for visual processing. As an attempt to use the whole omni-directional image and also resolve the distortion problem, Su and Grauman [16]

and Tateno *et al.* [19] used distortion-aware kernels at each latitude of the omni-directional image to take into account of the image resolving power variation. To tackle the distortion problem from tilting the camera, Bourke [1] proposed a way to postprocess the ERP image, but it would require knowledge regarding the camera orientation. Our method replaces the ERP-based representation as a way to tackle the distortion problems raised from ERP images.

2.2. Other representations for 360° images

As a way to represent spherical geometry, a few methods have been proposed to project an omni-directional image onto a cube to generate a cube map. The method in [12] utilizes a cube map to generate a saliency map of the omnidirectional image. As an extension to [12], Cheng et al. [3] proposed padding each face with pixels from tangent faces to consider information from all tangent faces and to convolve across the edges. Figure 3 shows an example of such a cube padding method. Utilizing a cube map projection of omni-directional images resolves many of the issues that ERP based methods faces. However, in cube map representation, there still exists noticeable variance of spatial resolving power between centers and edges of the cube faces. To address this variance of spatial resolving power, Brown [2] proposed the equi-angular cube (EAC) projection, changing the method in which omni-directional views are sampled onto a cube. Another representation that aimed to resolve the problems raised in the ERP representation was proposed in [4]. Cohen et al. [4] suggested transforming the domain space from Euclidean S^2 space to a SO(3) 3D rotation group to reduce the negative effects of the ERP representation.

Through its approximation of the spherical geometry, cube map projection has remedied the flaws of ERP to some extent: cube map projection does not suffer from severe distortion near the poles, it does not require the image to be constrained rotationally, and there is no discontinuity at the edges. While cube map projection negate many of the flaws in ERP based methods, it still has spatial resolving power variance between the edges and centers of cube faces. Compared with the cube map projection, our method further minimizes the variance of the spatial resolving power.

3. Proposed method

To obtain a new representation of an omni-directional image, we project an omni-directional image onto an icosahedral spherical polyhedron. After the projection, we run the transformed image through a CNN structure. The advantage of using our representation over using ERP or any other representations is that ours has far less distortion on an input image.

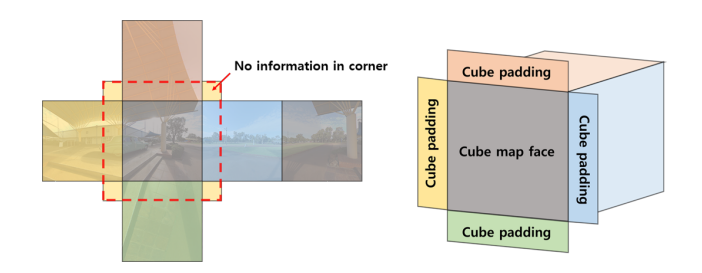


Figure 3. Cube padding allows the receptive field of each face to extend across the adjacent faces.

3.1. Definition of distortion

To discuss the distortion of omni-directional image representations, we need to define a quantitative measure of distortion. To do so we first define an effective area of a pixel for a given representation (i.e., ERP, cube map) as corresponding area when the pixel is projected onto a spherical polyhedron. The distortion of an omni-directional image representation can then be measured by the variation of pixels' effective areas. To compare the distortions for different representations, we define the average effective area of all the pixels in the given representation to be the geometric mean of them as shown in Eq. (1), where N is the total number of pixels and A_i is the i^{th} pixel's effective area.

$$A_{mean} = \sqrt[N]{\prod_{i=1}^{N} (A_i)} \tag{1}$$

Then, we define the distortion for i^{th} pixel, d_i , as a log scaled ratio of the individual pixel's area to their average, shown in Eq. (2).

$$d_i = \log(\frac{A_i}{A_{mean}})\tag{2}$$

Having defined the mean area to be the geometric mean, it can be shown that the log scaled ratios of distortions would always sum up to zero $(\sum_{i=1}^N d_i = 0)$. This is a desired behavior of distortion values because it is a measure of how much each individual pixel's effective area is deviated from the average of pixels' effective areas. We then define an overall distortion score for each representation as the root-mean-square of the distortions as

Distortion score =
$$\sqrt{\frac{1}{N} \sum_{i=1}^{N} d_i^2}$$
. (3)

3.2. Spherical polyhedron

Spherical polyhedrons are divisions of a sphere by arcs into bounded regions, and there are many different ways to construct such spherical polyhedrons. The cube map representation that was previously mentioned can be regarded

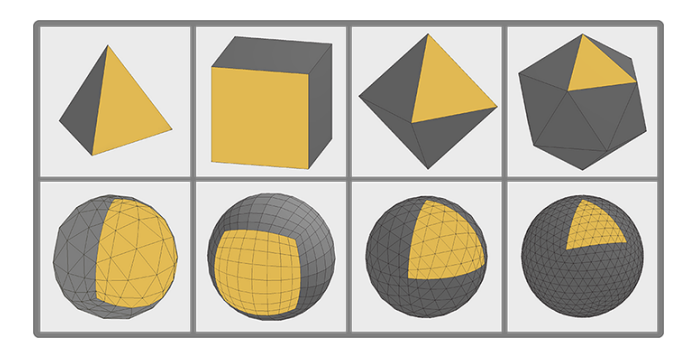


Figure 4. Subdivided pixel areas on 3^{rd} subdivision regular convex polyhedrons: tetrahedron, cube, octahedron, and icosahedron. The variance of pixel areas decreases with more equi-faced regions.

as an example of an omni-directional image projected onto a spherical polyhedron. The cube map representation splits the sphere into 6 equi-faced regions, creating a cubic spherical polyhedron; each of these 6 regions represents the faces of a cube. Similarly, we can apply such representation to other regular polyhedrons to create a spherical polyhedron that is divided into more equi-faced regions.

In the cube map representation, the squares of a cube are subdivided into smaller squares as to represent pixels in a cube map. The distortion of the cube map representation occurs when we create the cubic spherical polyhedron from a cube map: pixels in a cube map correspond to different areas on the cubic spherical polyhedron depending on the pixels' locations in the cube map. Here, when the squares on the cube are further subdivided into even smaller squares, the distortion score of the cubic spherical polyhedron converges early on ². It means that the distortion of a spherical polyhedron is more dependent on the initial geometry used to make the spherical polyhedron than the number of regular convex polyhedron face subdivisions. This suggests that a regular convex polyhedron with a greater number of faces can have lower distortion when it is subdivided and turned into a spherical polyhedron: so we use a regular polyhedron with the most faces, an icosahedron.

We can visually compare the variances in Fig. 4. A numerical table showing the variances of different spherical polyhedrons is included in the supplementary material.

3.3. Icosahedral spherical polyhedron (SpherePHD) representation

When creating a spherical polyhedron using an icosahedron, each subdivision subdivides each of the equilateral triangles into 4 smaller equilateral triangles.

Each of these subdivisions of triangles will be refered to as n^{th} subdivision where n refers to the number of times the triangles have been subdivided. After creating the sub-

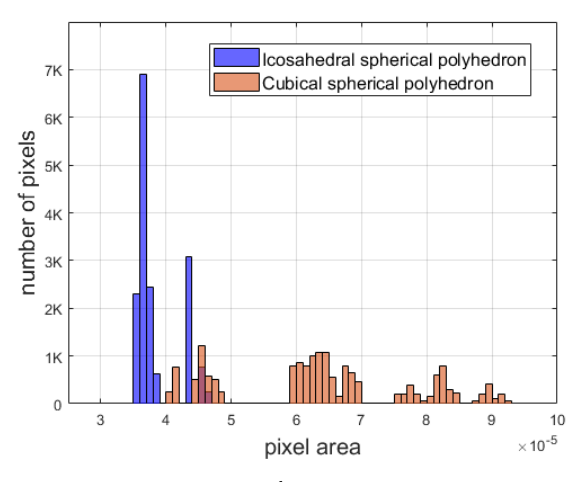


Figure 5. The pixel areas of 7^{th} subdivision icosahedral and cubical spherical polyhedrons on a unit sphere.

divided icosahedron, we extrude the newly created vertices from the subdivision onto a sphere, creating a geodesic icosahedron (note that the original vertices of the icosahedron already lie on a sphere). We can then create a spherical polyhedron through tessellation of this geodesic icosahedron onto a sphere. An example of these polyhedrons is shown in Fig. 6. A spherical polyhedron ³ constructed from a regular convex icosahedron has a small pixel area variance compared to the cubical spherical polyhedron as in Fig. 5.

Ultimately, we use this SpherePHD to represent omnidirectional images. To do so, we take an omni-directional image and project it onto this SpherePHD through one-to-one correspondence. We can do so because both omnidirectional images and the SpherePHD can be described in the same geometry. In this projection, the visual images will be represented by the individual triangles tessellated on the SpherePHD. Our SpherePHD representation results in much less variance of effective pixel areas compared with the cube map representation. The minimal variance of effective pixel areas would mean that our representation will have less variance in resolving power than the cube representation, leading to less distortion score.

Because the SpherePHD was made from a rotationally symmetric icosahedron, the resulting SpherePHD will also have rotationally symmetric properties, making this representation less affected by rotation. In addition, as the projection is a linear transformation, our method will not have any sinusoidal fluctuation effects like those seen in the ERP representation, making our representation more robust to rotation.

²The distortion table will be included in the supplementary materials

³The mentioning of spherical polyhedron throughout this paper will refer specifically to the icosahedral spherical polyhedron (SpherePHD) constructed through an geodesic icosahedron, unless specified otherwise

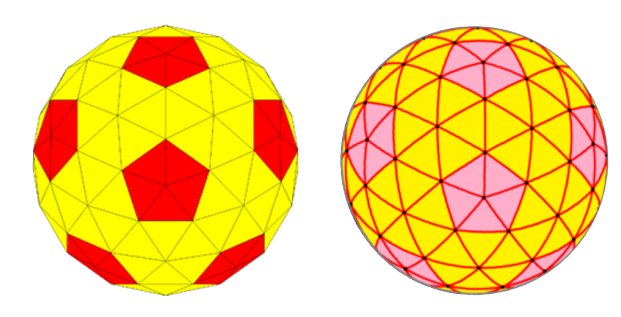


Figure 6. The polyhedron on the left is an example of icosahedral geodesic polyhedron. The polyhedron on the right is the SpherePHD version of the given geodesic icosahedron. Image is from [21]

3.4. SpherePHD convolution and pooling

The conventional CNNs compute a feature map through each layer based on a convolution kernel across an image. In order to apply CNNs to SpherePHD, it is required to design special convolution kernels and pooling kernels that meet certain criteria:

- 1. The convolution kernel should be applicable to all pixels represented in the SpherePHD and retain locality information of each pixel and its neighbors.
- 2. Applying the kernels through subsequent layers should provide the locality information of a pixel to other areas of the SpherePHD.
- 3. The convolution kernel should take into account that adjacent triangles are in different orientations.
- 4. The pooling kernel should reduce the image from a higher n^{th} subdivision to a lower $(n-1)^{th}$ subdivision of the SpherePHD.

To meet the first condition, our kernel needs to be a collection of triangles as our SpherePHD has triangular pixels. Another fulfillment that our kernel needs to meet is that it must be applicable to the 20 vertex points that are connected to 5 triangles while still being applicable to all the other vertex points connected to 6 triangles. For this reason, the vertices of the kernel should not be connected to more than 5 triangles; if the vertices are connected to more than 5 triangles, those vertices would not be able to convolve at the triangles connected to the 20 original icosahedron's vertices. Kernels fulfilling these requirements will meet the first condition.

To satisfy the second condition, the triangular pixel that is being convolved should be at the center of the kernel. If not, the pixel of interest will be assigned the convolution output of a neighboring pixel located at the center of the kernel.

Concerning the third condition, because triangular pixels adjacent to each other in our SpherePHD are oriented dif-



Figure 7. From left to right: proposed pooling kernel shape, the same pooling kernel applied onto adjacent triangle, proposed convolution kernal shape, the same convolution kernel applied onto adjacent triangle, and the convolution kernel meeting the requirement of criterion 1. The proposed kernels meet criterion 3 as the adjacent triangles orientation can also use the same kernel

ferently, we must design a kernel that can be applied to each of the triangles in their respective orientations.

For the last condition, the pooling kernel should be shaped so that the n^{th} subdivision polyhedron can be downsampled into the smaller $(n-1)^{th}$ subdivision polyhedron. To design such a pooling kernel, we reverse the method in which the subdivisions are formed: we pool 4 smaller triangles into a single triangle.

Our convolution kernel and pooling kernel meet the above criteria are given in Fig. 7.

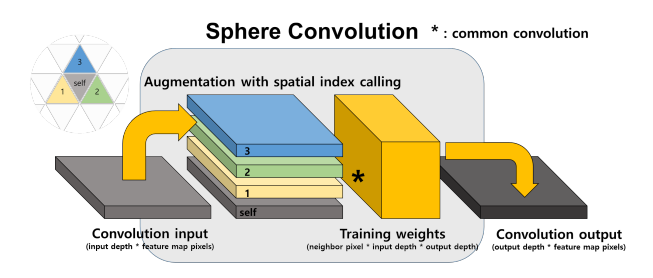
The pooling kernel is dependent on how the triangles are subdivided in the construction process. For example, if we subdivided a triangle into n^2 smaller triangles, we can use a pooling kernel that takes the same n^2 smaller triangles to form one larger triangle. However, for simplicity we subdivided a triangle into 4 smaller triangles.

In Fig. 7, we propose that our kernels can be used for adjacent triangles with different orientation. As we convolve across the SpherePHD image, the convolution kernel is flipped 180° when applied to the next adjacent triangle. We propose that this flipping enables the kernel to learn rotation invariant features.

3.5. CNN Implementation

Utilizing our representation from Sec. 3.3 and our kernels from Sec. 3.4, we implement a CNN for omnidirectional images. In each of the layers of the CNN, we convolve the SpherePHD representation of an omnidirectional image with the proposed kernels by iterating in a spiral manner through the SpherePHD. After convolution, we perform a pooling with the resulting feature map using our pooling kernel. Due to our SpherePHD representation and our kernels, a convolution-pooling layer will have one less subdivision e.g. the n^{th} subdivision SpherePHD will be the $(n-1)^{th}$ subdivision SphedPHD after a layer of convolution-pooling. Depending on the format of the desired output, we can adjust how much we reduce the number of subdivision.

Convolution layer The SpherePHD image that we use has a specific indexing system, laid out as a 1-D tensor, to call each of the triangular pixels. To call on the adjacent triangular pixels in the convolution kernel, we stack 1-D ten-



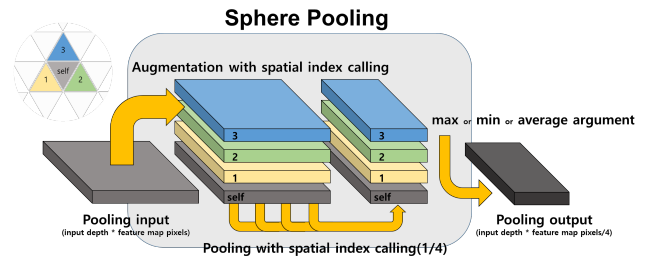


Figure 8. Tensor-wise representation of our implementation of convolution and pooling layers that we proposed.

sors of indices which call on the adjacent triangular pixels. The now 2-D tensor contains indices of triangular pixels, in order of the local triangular pixel and the corresponding pixels in its convolution kernel. We then replace the indices with the corresponding color or feature map. As a result, we get a 3-D tensor that has dimensions of [number of triangular pixels, input depth, kernel location]. We can convolve this 3-D tensor with weights of size [kernel size, 1, input depth, output depth]. This results in the output having a size of [number of triangular pixels, output depth]. Figure 8 shows a graphical representation of this convolution.

Pooling layer Implementing the pooling layer is much similar to implementing the convolution layer in that we use the same stacking method to call upon the corresponding pixels and apply the desired pooling operation. This pooling layer is also shown in Fig. 8.

3.6. Limitation of polyhedron approaches

One of the limitations of our proposed SpherePHD approach is that the current convolution kernel strides in a spiral manner through the SpherePHD. This spiral method causes convolution kernels to constantly experience distortion as the kernel strides around the poles. This can reduce our accuracy closer towards the poles.

4. Experiments

We evaluate our method and also compare with existing methods that use ERP and cube map representation [3] on MNIST [6] classification and SYNTHIA [15] vehicle detection tasks. To show the feasibility and the effectiveness of using the proposed SpherePHD representation, we compare classification performance with MNIST images randomly



Figure 9. From left to right: ERP, Cube map, SpherePHD representations. These are the three different types of input images. All images represent MNIST digit 5.

projected on SpherePHD, cube, and equi-rectangular plane with directional information. We also present a simple network based on the proposed method for the SYNTHIA vehicle detection task to demonstrate the versatility of the proposed method to other detection networks.

4.1. MNIST classification

Dataset We made 3 types of spherical MNIST dataset by projecting original 70k MNIST dataset images onto SpherePHD, cube map, and equi-rectangular plane like Fig. 9. Original MNIST images were randomly positioned and oriented on the sphere surface. However, training set and test set differ in their position distributions. Training set was made to have uniform distribution on the sphere surface, while test set was made to have uniform distribution along their longitude and latitude. In the latter case, the images are more likely to be found on the poles of the sphere, making it different from having uniform distribution on the sphere surface. We made the train and test set differently because when training the network the images should be found uniformly over the sphere surface, but when testing, we wanted to evaluate the results and compare them with the distortion distribution in terms of longitude and latitude. We augmented training data from 60k to 1,200k because random position and random orientation of digits greatly increase the degree of freedom of the task. We also augmented test data from 10k to 700k. This is not a normal train-test set ratio, but it is for achieving robust accuracy distribution with low standard deviation in Fig. 11.

We decided the image size of SpherePHD image to 3 times subdivided size which is $1 \times 1280 (= 20 \times 4^3)$ to maintain similar resolution with 28×28 original MNIST images. To unify the spatial resolving power of all datasets, the sizes of cube map and ERP images were adjusted based on the equator pixels of the SpherePHD image. The number of pixels along the equator of all datasets is same and sizes are 40×80 for ERP image and $6 \times 20 \times 20$ for cube image.

A field of view (FoV) of projection is 60°, which is bigger than FOV of a SpherePHD face (42°) and smaller than FoV of a cube map face (90°). This condition makes MNIST digits include enough variance of distortion.

Implementation details We designed the single neural network as fully convolutional structure for all three

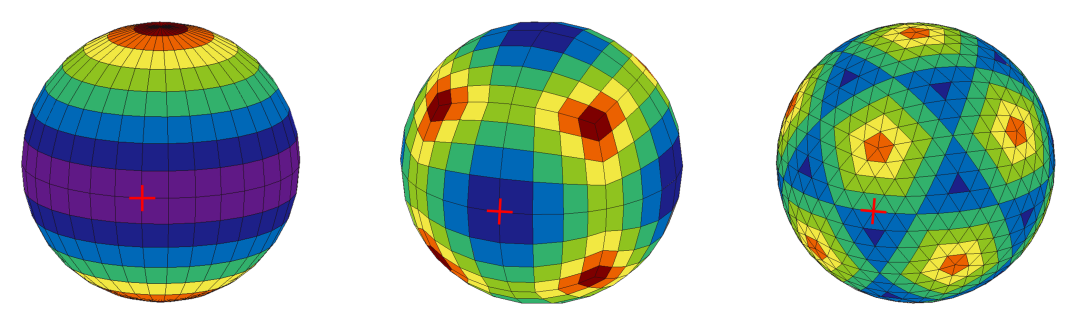


Figure 10. Distribution of distortion values defined in Sec. 3.1. The red cross mark represents 0 latitude and 0 longitude point on a sphere surface.

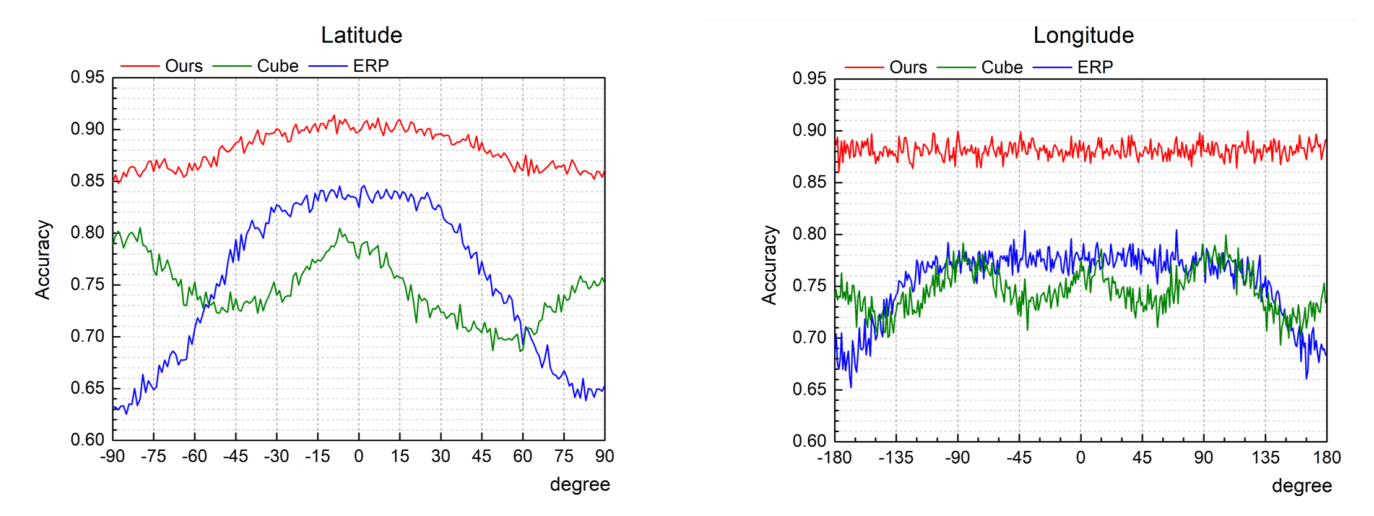


Figure 11. MNIST classification accuracy of 700k test set along latitude and longitude. The number of samples along latitude and longitude follows uniform distribution. This result highly related with distortion along latitude and longitude. Fig. 10

datasets. It has 2 pairs of a convolution layer and a max pooling layer followed by a pair of a convolution layer and a global average pooling layer. The convolution layers with a max pooling layer extract features while the convolution layer with a global average pooling layer predict the class.

To compare the performance with same structure and same parameter scale, we used global average pooling layer inspired by NiN [10] for classification instead of fully connected layer. Due to the fully convolutional structure, the parameter scale of this network is independent to the input image size. It is only dependent to the convolution kernel size and we also minimized the difference of kernel sizes by using 10×1 kernel in our method and 3×3 kernel in other methods.

Result To evaluate our method compared with other baselines, we compare the MNIST classification performance with the longitude and latitude for SpherePHD, cube, and ERP images. The classification accuracy for three datasets is shown in Fig. 11. First, when comparing the latitude-wise results, we can see that the proposed method shows uniform accuracy in the low latitude regions near 0°

and slightly reduced accuracy in the high latitude regions near -90° and 90°. On the other hand, the ERP method presents noticeable reduction of accuracy in high latitude regions and the cube map method presents periodic reduction of accuracy with 90° interval. These results are highly related with distribution of the distortion values shown in Fig. 10. Overall accuracy distribution follows the variation of the distortion values in the local window. When the window is applied to a region with severe distortion variation, low quality information is supplied to the network, which causes performance degradation. As shown in Fig. 10, the regions where the distortion variation is large like edge and vertex matches well with the regions where the accuracy decreases. Additionally, we can expect a gradual degradation of accuracy near the poles because of the way our kernel strides, as mentioned in Sec. 3.6. Second, when comparing the longitude-wise results, we can also see accuracy distribution matching well with the distortion variation. However the result of our method does not show gradual accuracy degradation because the effect of kernel alignment is evenly distributed to all longitude. The ERP method has almost uniform accuracy distribution and cube map method shows low accuracy in the parts where distortion variation is large. Exceptionally, the ERP method presents significant accuracy drop due to discontinuity of the ERP image boundary.

4.2. SYNTHIA vehicle detection

Dataset SYNTHIA dataset is a vitrual road driving image dataset [15]. Each sequence in the dataset consists of front, right, left, and back NFoV images of a driving vehicler, along with the ground truth labels for each object in each scene. Since the camera centers for the four directions are the same at a given moment, we can make a 360° image for the scene. We projected the scene onto ERP and SpherePHD representation. While projecting them, we tilted the horizon randomly relative to the the equator of ERP or SpherePHD. We augmented each scene to be three-fold by assigning different random orientations for the horizon relative to the equator. We made the resolution for the ERP and SpherePHD images to be 1280×2560 and 20×4^8 each. These resolutions were selected to make them have the same number of pixels on their equators.

Implementation details Using the labeled ground truth, we performed vehicle detection test using SpherePHD and ERP representation. To compare the detection accuracy between the two methods fairly, we performed the experiment using similar CNN architectures (based on YOLO [13]) having the same depth. We used shallow networks to see the difference between the two networks in terms of their learning capability using constrained number of parameters. We implemented the network on our dataset by dividing the input image into S grids, where $S = 320 (= 20 \times 4^2)$ for the network using our method, and $S = 325 (= 13 \times 25)$ for the ERP method. We tried to make the size of the output layers the same for both networks as it is critical for the detection performance in networks based on YOLO. Also, as we only wanted to test the feasibility of our representation, we reduced the complexity of detection by using bounding circles instead of bounding boxes. As a result, the network is to predict 4 values for each grid: probability P of the existence of an object in the grid, x and y for the position of the object relative to the grid, and radius r of the bounding circle. The overall output of the network is a $S \times 4$ tensor.

The modified YOLO loss used for our experiment is defined as follows

$$\lambda_{coord} \sum_{i=0}^{S} [(x_i - \hat{x}_i)^2 + (y_i - \hat{y}_i)^2 + (r_i - \hat{r}_i)^2] + \sum_{i=0}^{S} (P_i - \hat{P}_i)^2 + \lambda_{noobj} \sum_{i=0}^{S} (P_i - \hat{P}_i)^2$$
(4)

Where we put the weights on each term of the loss as $\lambda_{coord} = 5$ and $\lambda_{noobj} = 0.5$, by the same reason as YOLO.



Figure 12. Tilted 360° SYNTHIA dataset images projected on ERP (upper) and SpherePHD (lower) with corresponding ground truth(left) for the vehicle detection(right). GT(left) and detection results(right) are represented as circles in ERP images (upper) and spheres in SpherePHD images (lower).

Result The network for our method started to converge easily, while it was difficult to make the network using ERP representation converge. As can be seen in Fig. 12, the detection using ERP representation completely fails to detect vehicles using the shallow network. On the other hand, the network using our method was able to detect and localize the vehicles. The proposed network is expected to perform better if it was trained more since it has not converged yet. Because of the severe distortion of the ERP representation towards the poles, the shallow network we used seems to be incapable of dealing with the detection task using ERP representation. Conversely, using our method the network was able to detect vehicles since the SpherePHD has far less distortion. More of our experimental results will be provided in the supplementary materials.

5. Conclusion and future works

Despite several advantages of 360° images, CNNs have not been successfully applied to 360° images due to the problems, such as shape distortion due to nonuniform resolving power and loss of continuity, raised from the representation method for 360° images. To resolve those problems, we have proposed a new image representation for omni-directional images. The proposed representation is based on the SpherePHD derived from an icosahedron and has less distortion than ERP or cube map representations. To apply CNNs to 360° images using the proposed representation, we also proposed SpherePHD convolution and pooling methods. Finally, we have provided implementation details to apply the proposed method to existing CNNbased methods, and also demonstrated the feasibility and efficacy of the proposed method through both classification and detection tasks using the MNIST and sphrical SYN-THIA datasets.

In the future, we will create a real world 360° dataset to test our representation on real world images instead of

synthetic ones. Furthermore, we will find a more suiting bounding area definition to increase detection accuracy.

References

- [1] P. Bourke. Converting an equirectangular image into another equirectangular image. http://paulbourke.net/miscellaneous/sphere2sphere/, 2017. 2, 3
- [2] C. Brown. Bringing pixels front and center in vr video. https://blog. google/products/google-ar-vr/ bringing-pixels-front-and-center-vr-video/, 2017. 3
- [3] H.-T. Cheng, C.-H. Chao, J.-D. Dong, H.-K. Wen, T.-L. Liu, and M. Sun. Cube padding for weakly-supervised saliency prediction in 360 videos. In *The IEEE Conference on Computer Vision and Pattern Recognition (CVPR)*, June 2018. 3, 6
- [4] T. S. Cohen, M. Geiger, J. Köhler, and M. Welling. Spherical cnns. In arXiv preprint arXiv:1801.10130, 2018. 3
- [5] B. Coors, A. Paul Condurache, and A. Geiger. Spherenet: Learning spherical representations for detection and classification in omnidirectional images. In *The European Conference on Computer Vision (ECCV)*, September 2018. 2
- [6] L. Deng. The mnist database of handwritten digit images for machine learning research [best of the web]. *IEEE Signal Processing Magazine*, 29(6):141–142, 2012. 6
- [7] H.-N. Hu, Y.-C. Lin, M.-Y. Liu, H.-T. Cheng, Y.-J. Chang, and M. Sun. Deep 360 pilot: Learning a deep agent for piloting through 360 sports videos. In *Proc. CVPR*, pages 1396–1405, 2017.
- [8] A. Krizhevsky, I. Sutskever, and G. E. Hinton. Imagenet classification with deep convolutional neural networks. In F. Pereira, C. J. C. Burges, L. Bottou, and K. Q. Weinberger, editors, *Advances in Neural Information Processing Systems* 25, pages 1097–1105. Curran Associates, Inc., 2012. 1
- [9] W.-S. Lai, Y. Huang, N. Joshi, C. Buehler, M.-H. Yang, and S. B. Kang. Semantic-driven generation of hyperlapse from 360 degree video. *IEEE transactions on visualization and* computer graphics, 24(9):2610–2621, 2018. 2
- [10] M. Lin, Q. Chen, and S. Yan. Network in network. arXiv preprint arXiv:1312.4400, 2013. 7
- [11] D. Maturana and S. Scherer. Voxnet: A 3d convolutional neural network for real-time object recognition. In *IEEE/RSJ International Conference on Intelligent Robots and Systems*, page 922–928, September 2015. 1
- [12] R. Monroy, S. Lutz, T. Chalasani, and A. Smolic. Salnet360: Saliency maps for omni-directional images with cnn. *Signal Processing: Image Communication*, 2018. 2, 3
- [13] J. Redmon, S. Divvala, R. Girshick, and A. Farhadi. You only look once: Unified, real-time object detection. In *The IEEE Conference on Computer Vision and Pattern Recogni*tion (CVPR), June 2016. 1, 8
- [14] S. Ren, K. He, R. B. Girshick, and J. Sun. Faster R-CNN: towards real-time object detection with region proposal networks. *CoRR*, abs/1506.01497, 2015.

- [15] G. Ros, L. Sellart, J. Materzynska, D. Vazquez, and A. M. Lopez. The synthia dataset: A large collection of synthetic images for semantic segmentation of urban scenes. In *The IEEE Conference on Computer Vision and Pattern Recognition (CVPR)*, June 2016. 2, 6, 8
- [16] Y.-C. Su and K. Grauman. Learning spherical convolution for fast features from 360 imagery. In *Advances in Neural Information Processing Systems*, pages 529–539, 2017.
- [17] Y.-C. Su and K. Grauman. Making 360 video watchable in 2d: Learning videography for click free viewing. arXiv preprint, 2017. 2
- [18] Y.-C. Su, D. Jayaraman, and K. Grauman. Pano2vid: Automatic cinematography for watching 360 videos. In Asian Conference on Computer Vision, pages 154–171. Springer, 2016. 2
- [19] K. Tateno, N. Navab, and F. Tombari. Distortion-aware convolutional filters for dense prediction in panoramic images. In *The European Conference on Computer Vision (ECCV)*, September 2018. 3
- [20] Y. Wenyan, Q. Yanlin, C. Francesco, F. Lixin, and K. Joni-Kristian. Object detection in equirectangular panorama. arXiv preprint arXiv:1805.08009, 2018. 2
- [21] Wikipedia contributors. Geodesic polyhedron Wikipedia, the free encyclopedia, 2018. [Online; accessed 15-November-2018]. 5
- [22] J. Xiao, K. A. Ehinger, A. Oliva, and A. Torralba. Recognizing scene viewpoint using panoramic place representation. In 2012 IEEE Conference on Computer Vision and Pattern Recognition, pages 2695–2702, June 2012.